Progress in Propulsion Physics **11** (2019) 295-316
https://doi.org/10.1051/eucass/201911295

NONLINEAR ANALYSIS OF LOW-FREQUENCY COMBUSTION INSTABILITIES IN LIQUID ROCKET ENGINES

M. Leonardi[1], F. Di Matteo[2], J. Steelant[2], F. Nasuti[1], and M. Onofri[1]

[1]University of Rome "La Sapienza"
18 Via Eudossiana, Rome 00186, Italy
[2]ESA-ESTEC
1 Keplerlaan, Noordwijk 2201 AZ, The Netherlands

Low-frequency combustion instabilities are here studied taking advantage of the software EcosimPro. A specific module has been implemented based on the double time lag model and the coupling of combustion chamber and feed line oscillations were investigated by using a complete set of nonlinear equations. The characteristic time lags have been identified following two approaches: (*i*) a constant time lag approach; and (*ii*) a variable time lag approach based on correlations available in open literature. To prove the module capabilities, an experimental setup was reproduced and a stability map was generated, comparing the obtained results with literature data from both experiments and a linear double time lag model. The stability boundaries obtained with the chugging module are in good agreement with those obtained in open literature and the first characteristic frequency of the engine is well predicted. Furthermore, the model proves its capability in reconstructing the reversal in the slope of the stability boundary at low fuel injector pressure drops and in detecting the high-frequency content typically observed in presence of multimode oscillations. However, in the calculations, the higher frequency does not dominate the instabilities, that is, in the unstable regime, the model diverges with a frequency equal to the first characteristic frequency. In the last part of the paper, the variable time lag approach is used to investigate a portion of the aforementioned stability map. Thanks to the semiempirical correlations, the present authors managed to improve the prediction of the first characteristic frequency, whereas the stability boundary does not change significantly and remains comparable with the one predicted by the constant double time lag approach.

NOMENCLATURE

A	cross-section area
E	total energy
H	total enthalpy
MR	mixture ratio
p	pressure
R	gas constant
T	temperature
t	time
u	velocity
V	volume
x	axial coordinate
Δp	injector pressure drop
ξ	pressure drop coefficient
ρ	density
atom	atomization
c	chamber
crit	critical conditions
fu	fuel
g	gas
l	liquid
nc	noncondensable
ox	oxidizer
pw	powder gases
th	throat
vap	vaporization

1 INTRODUCTION

In this paper, a numerical analysis of low-frequency combustion instabilities, frequently referred to as chugging, in Liquid Rocket Engine (LRE) is proposed taking advantage of an unsteady nonlinear approach. Low-frequency combustion instabilities in LREs are characterized by oscillations in the mass flow rate of propellants that result in pulsations of the chamber pressure. The response of the combustion chamber to the upstream oscillations is not immediate. The delay is due to the different characteristic times associated with the processes of injection, atomization, vaporization, mixing, and combustion, taking place in quick succession inside the combustion chamber. Moreover, the

mass flow rate is not immediately responsive to pressure oscillations because of the propellant inertia in the feed lines. Hence, both feed lines and combustion chamber physics must be taken into account. Low-frequency instabilities have been usually investigated with the help of linearized models [1–5], whereas only a few attempts have been made to detail the phenomena with nonlinear models [6, 7]. In the present study, an unsteady nonlinear analysis of chugging instabilities is proposed with particular attention to the appropriate modeling of delays induced by atomization, vaporization, and mixing processes.

The analysis of chug instabilities requires to model the subsystems of an LRE to investigate the mutual influence of each component. Such a comprehensive simulation inherently needs simplified submodels able to give a satisfactory level of reliability along with a reasonable computational time. In this context, an object oriented simulation tool is a valid option to handle the complexity of a propulsion system. EcosimPro [8] is a simulation platform focused on the analysis of complete systems that spans different engineering fields. Thanks to the object oriented philosophy, single components can be connected to each other in order to analyze systems at different complexity levels. Propulsion systems can be investigated by the European Space Propulsion System Simulation (ESPSS) library [9, 10], in which the typical components of an LRE (tanks, turbomachinery, feed lines, valves, gas generator/preburner, combustion chamber, etc.) are modeled to study both steady-state and transient phases.

To detect low-frequency instabilities, it is important to properly model the characteristic times associated with both liquid and gases injected into the combustion chamber. Chug instabilities arise when the total time lag is such that oscillations in the rate of propellant injection are coupled with the corresponding oscillations of the chamber pressure. Different studies have been performed during the past decades to investigate which time lag is the most important for the generation of low-frequency instabilities. Most of the proposed chug models focused on steady linear analyses are based on the linearization of the continuity equation in the combustion chamber. In the attempt of explaining damages caused by chugging in LRE, Gunder and Friant [1] introduced the time lag concept. They linearized the energy conservation equation and solved the relative delay differential equation. The time lag approach was further extended by Summerfield [2] who retrieved a stability analysis from the linearization of the continuity equation introducing the influence of the feed lines. He investigated the effects of feed lines, injector pressure drops, and combustion chamber length on chug instabilities.

A comprehensive theoretical approach based on the concept of sensitive and insensitive time lag was then proposed by Crocco and Cheng [3, 11, 12]. Their approach is based on the concentrated combustion model and applies to both monopropellant and bipropellant cases. Later, Wenzel and Szuch [4, 13–15] developed a model that incorporates a double time lag approach, hence extending

the potentialities of the original Crocco's model to the cases in which the two propellants have different time lags. They applied the model to analyze a system ignoring the influence of the feed lines and considering only the injector impedances. They used a useful engineering approach to express the solutions, highlighting the importance of injector pressure drops on instabilities. Recently, Casiano [5] extended the Wenzel and Szuch's model by formulating the problem in a parametric form and adding the influence of the feed lines. Linear models have been also developed to study Pogo instabilities that are combustion instabilities characterized by the coupling of combustion and structural dynamics and that usually bring to structural as well as to thrust oscillations. Pogo instabilities arise at low frequencies well below 100 Hz, thus making Pogo models appealing for the study of chug instabilities. Such is the case of Ordonneau *et al.* work, where a Pogo model, originally meant to study Pogo instabilities in the VULCAIN engine, has been adapted to both analyze chug instabilities of VULCAIN and predict those of VULCAIN 2 engine [16, 17]. Beside these linear approaches, a few attempts have been made in the field of nonlinear analysis, mainly because the computational cost of such approaches was too high for the hardware resources. Webber's [6] work was the first attempt of performing an unsteady analysis based on nonlinear equation for both the feed lines and the combustion chamber. He focused his attention towards the modeling of the liquid phase in the combustion chamber, showing the effects of droplet sizes on the amplitude of the low-frequency oscillations. Bartrand [7] proposed an extension of this model, including the effects of finite rate chemistry and showed that in the Space Shuttle Main Engine preburner case, the assumption of finite combustion velocity affects the magnitude of the damping rather that the frequency of oscillations.

The analyses conducted in this paper take advantage of the ESPSS feed lines modeling approach, whereas the combustion chamber component is suitably improved by means of a chug dedicated module. It is well known that the shift, or time lag, between disturbances coming from injectors and pressure response is the sum of five time lags [18], each related to a specific process taking place in the combustion chamber. The five processes are, in order: injector response, atomization, vaporization, mixing, and combustion. It is commonly accepted that the most important delays are those related with atomization, vaporization, and mixing [7, 19], whereas spatial droplet distribution produced by injection has been shown to have a great effect on high-frequency instabilities but has a little or no effect on chugging [15]. Moreover, in the case of liquid oxygen and gaseous hydrogen propellant combination, combustion can be considered faster than other processes and the related time lag can be ignored. On the contrary, the vaporization rate is of great importance for the evaluation of chugging and is strictly related with the atomization process (droplet size and surface area). Therefore, the present authors focus their attention on atomization, vaporization, and mixing phenomena. Two different approaches

are foreseen: a constant time lag approach and a variable time lag approach. In the constant approach, both atomization and mixing time lag remains unchanged throughout the entire simulation. Instead, for the variable approach both atomization [20] and vaporization [20, 21] will be modeled with the aim of semiempirical correlations while mixing times will be retrieved from an empirical curve [14]. In this way, the characteristic times depend on the main combustion chamber parameters, thus changing during the simulation. The chug module with the two approaches will be validated against experimental and numerical data available in open literature [22] and the differences between the two methods will be discussed.

2 NUMERICAL METHOD AND APPROACH

The LRE system is here modeled with EcosimPro, taking advantage of the components included in the ESPSS library, for which a complete description can be found in different works [9, 10, 23]. In the following, the feed lines and injector components are briefly introduced, whereas more details are provided for the combustion chamber component. The modeling approach for the gas phase in the combustion chamber is particularly important for the scope of the present paper, because it is the frame in which the vaporization, atomization, and mixing models are included.

2.1 System Components

2.1.1 Feed line and injector components

The tube component is modeled with a quasi-one-dimensional, unsteady approach for two phase flow. The two phase flow evolution is described by the Homogeneous Equilibrium Model (HEM) [24], which is based on two assumptions:

(1) thermodynamic equilibrium between the two phases; and

(2) same velocity for both liquid and vapor.

Thanks to these hypothesis of flow in equilibrium, it brings to a set of equations whose structure is close to the Euler equations and, more importantly, that are unconditionally hyperbolic. The two-phase fluid can be either a simplified liquid or a real fluid. The governing equations consider one continuity equation for the noncondensable perfect gas, one for the noncondensable perfect gas diluted in the liquid phase, one for the overall mixture, one momentum equation, and one

energy equation for the overall mixture. The set is completed by N equations, one for each of the chemical species convected in the pipe. These latter continuity equations are needed when the pipe is located downstream of a component in which reactions take place, e. g., preburner and gas generator, and the convection of the combustion gases must be taken into account. It is worth noticing that both the noncondensable gas and the two-phase fluid can be two different real fluids, whose properties are retrieved from a dedicated database. Different flow mixture configurations are possible, e. g., pure liquid, liquid and vapor, and vapor and noncondensable. Therefore, flow properties must be calculated according to the mixture state and proper mixing rules have to be adopted.

Injectors and injector cavities are located between the feed lines and the combustion chamber. Injector cavities are modeled by means of a two-phase set of equations for a nonadiabatic variable volume. Two mass conservation equations and one energy equation describe the evolution of the two-phase mixture. The velocity in the cavity is calculated as an average velocity retrieved from the mass flow rate of the incoming fluid (calculated by the tube component) and the fluid going to the combustion chamber (calculated by the injector component); hence, no momentum equation is solved. Finally, the injector component is based on a momentum equation and calculates the mass flow across the injector in both turbulent and laminar regimes. The momentum equation accounts for concentrated pressure losses and for the inertia associated with the connected components. Once the mass flow rate is known, the energy flux is simply calculated as the product of the injector mass flow rate and the stagnation enthalpy of the fluid in the upstream cavities. In this way, both mass and energy fluxes are provided to the combustion chamber component.

2.1.2 Combustion chamber

The thrust chamber component consists of two subcomponents. The first one is an unsteady component that models the combustion chamber up to the throat. In this part of the combustion chamber, the flow is considered either in chemical equilibrium or in a "time delayed" equilibrium state that is a simple approach mimicking finite rate models. In the present analyses, we will consider the component as based on the chemical equilibrium assumption. Instead, the divergent part is a quasi-steady component that mimics the supersonic expansion by means of analytical correlations for a flow in either frozen or equilibrium conditions.

The first part of the combustion chamber is based on a quasi-one-dimensional formulation of the governing equations. The component is nonadiabatic, hence allowing for thermal connections with the external components, i. e., cooling channels. The unsteady conservation equations are:

$$\frac{\partial \boldsymbol{u}}{\partial t} + \frac{\partial \boldsymbol{f}(\boldsymbol{u})}{\partial x} = \boldsymbol{S}(\boldsymbol{u})$$

with

$$\left.\begin{aligned}
\boldsymbol{u} &= A\rho \begin{pmatrix} 1 \\ x_{\mathrm{fu}} \\ x_{\mathrm{ox}} \\ x_{\mathrm{pw}} \\ x_{\mathrm{nc}} \\ u \\ E \end{pmatrix} ; \qquad \boldsymbol{f}(\boldsymbol{u}) = A\rho \begin{pmatrix} uA \\ x_{\mathrm{fu}}uA \\ x_{\mathrm{ox}}uA \\ x_{\mathrm{pw}}uA \\ x_{\mathrm{nc}}uA \\ \left(u^2 + \dfrac{p}{\rho}\right) A \\ uHA \end{pmatrix} ; \\
\boldsymbol{S}(\boldsymbol{u}) &= \begin{pmatrix}
\dfrac{A\ (\dot{m}_{\mathrm{vap,fu}} + \dot{m}_{\mathrm{vap,ox}})}{V} \\
\dfrac{A\ (\dot{m}_{\mathrm{vap,fu}} - \dot{m}_{\mathrm{bu}} x_{\mathrm{fu}})}{V} \\
\dfrac{A\ (\dot{m}_{\mathrm{vap,ox}} - \dot{m}_{\mathrm{bu}} x_{\mathrm{ox}})}{V} \\
\dfrac{A\ -\dot{m}_{\mathrm{bu}} x_{\mathrm{pw}}}{V} \\
\dfrac{A\ -\dot{m}_{\mathrm{bu}} x_{\mathrm{nc}}}{V} \\
-\dfrac{1}{2}\dfrac{d\xi}{dx}\rho u\,|u|\,A + p\left(\dfrac{dA}{dx}\right) \\
\dfrac{\delta\dot{q}_w}{dx} + \dfrac{\delta\dot{q}_{\mathrm{unst}}}{dx} + \dot{m}_{\mathrm{vap}}\Delta q_{\mathrm{vap}}
\end{pmatrix}
\end{aligned}\right\} \qquad (1)$$

where ρ must be intended as the density of the mixture of gases and the subscript 'bu' refers to the burned gases that are calculated only when the "time delayed" rate approach is used. No further details are here given on these terms since we do not use such a modeling approach. The first source term on the right-hand side of the momentum equation models the friction effects, while the second is related to the effects of a variable area. The first source term in the energy equation $\dot{q}_w$ is the heat exchanged with the combustion chamber walls while the second term $\dot{q}_{\mathrm{unst}}$ is an excitation term introduced in the present analysis to mimic the roughness of the combustion processes. Finally, the vaporized mass source term in the continuity equation $\dot{m}_{\mathrm{vap}}$ is expressed according to the vaporization models described in the next section.

The nozzle component is a quasi-steady component able to describe the evolution of a flow in a duct with variable cross section. The nozzle takes the upstream thermodynamic state from the last computational cell of the combustion chamber and characterises the throat and the diverging section conditions. It should be noted that the modeling of the supersonic evolution is not directly needed to properly model chug instabilities since the only boundary condition that affects the detection of chug instabilities is the one giving the mass flow evolution at the throat section. However, the component is left in its original

formulation as the presence of the diverging nozzle does not limit the chug model capabilities.

2.1.3 Time lag approach

Once injected into the combustion chamber, the liquid subsequently undergoes atomization, vaporization, mixing, and combustion. The time lags of each process must, hence, be characterized in an appropriate way in order to catch the coupling between the feed lines and the combustion chamber. The general numerical procedure is the following: once injected in the combustion chamber, the mass associated with the liquid droplet is stored in a memory array and conserved for a time equal to the total time lag (vaporization, atomization, and mixing) associated with the droplet. After the ascribed time lag, the incoming mass is injected as a vaporized source term in the continuity equations (1). Two different cases are foreseen. In the first one, the time lags are user-defined input parameters and remain constant throughout the simulation. The second case is, instead, based on a time delayed approach in which the vaporization and atomization processes are described by time lags based on chamber conditions and liquid phase properties. The mixing times are retrieved from an empirical curve [14], while the combustion is considered as sufficiently fast and its time lag is neglected. In the present study, we decided to focus our attention towards the widely used oxygen–hydrogen combination, hence the correlations applied to the characteristic times hold only for this propellants. In particular, the hydrogen is injected in a gaseous phase; therefore, the delay characterizing this propellant is only the mixing time lag. The oxidizer is instead injected in a liquid phase; hence, it undergoes also vaporization and atomization. The time lags and the related parameters are calculated as follows. For the atomization processes, we apply the correlation [20]:

$$\tau_{\text{atom}} = 6 \cdot 10^{-4} \left(\frac{\rho_g}{\rho_l} \right)^{-0.32} \text{We}_g^{0.03} \text{Re}_l^{0.55} \frac{D_l}{u_l}$$

where

$$\text{Re}_l = \frac{u_l D_l \rho_l}{\mu_l}\,; \qquad \text{We}_g = 2\rho_g \frac{(u_g - u_l)^2 D_l}{\sigma_l}\,;$$

D_l is the liquid post inner diameter; u_l is the liquid velocity at injection; σ_l is the liquid surface tension; Re_l is the Reynolds number for the injected droplet; and We_g is the Weber's number for the combustion chamber gases.

Vaporization characteristic times for droplets when in presence of convection [20,25–27] are usually retrieved as a correction of those obtained for droplets

immersed in a quiescent gaseous environment [28]. We here make use of the correlation [20]:

$$\tau_{\text{atom}} = 6 \cdot 10^{-4} \left(\frac{\rho_g}{\rho_l} \right)^{-0.32} \text{We}_g^{0.03} \text{Re}_l^{0.55} \frac{D_l}{u_l} \,; \tag{2}$$

$$\tau_{\text{vap}} = \frac{\tau_{\text{vap,Re=0}}}{1 + 1.5\alpha} \,, \qquad \alpha = 1 - \frac{0.3 p_c}{100} \,; \tag{3}$$

$$\tau_{\text{vap,Re=0}} = \frac{D_0^2}{k} \,, \;\; k = 10^{-6} \left[1.01 \frac{1}{1 + \text{MR}} + 1.16 \cdot 10^{-3} \left(T_\infty - T_{\text{cr}} \right)^{0.93} \right]^{0.86}$$

where p_c is the chamber pressure; MR is the mixture ratio; T_∞ is the temperature of the combustion chamber gases; T_{cr} is the liquid critical temperature; and D_0 is the initial droplet diameter. The initial droplet diameter D_0 is here calculated from a correlation specifically developed for coaxial injectors and liquid oxygen [21]:

$$D_0 = C_{\text{inj}} K \cdot 127 \left(\frac{V_r}{160} \right)^{-0.93} \left(\frac{D_l}{2} \right)^{2.25} \left(\frac{D_g}{3} \right)^{-2.65} \left(\frac{R_{\text{post}}}{D_l} \right)^{-0.26} \tag{4}$$

with V_r being the relative velocity between injected liquid and gases in the combustion chamber, D_g the annular gap outer diameter, R_{post} the recess length, C_{inj} the parameter taking into account the injector design ranging from 0.4 to 1.2, and K the correction factor to be applied when the experimental simulants differ from the actual propellants [29].

3 TEST CASE

In order to prove the chugging module capabilities, let us refer to an experimental test case specifically developed to validate a linear double time lag model [22]. The experimental apparatus is a gaseous-hydrogen liquid-oxygen engine. The injector cavities and injector plate were specifically designed to ensure the desired pressure drops and a constant pressure in the injector cavities. The main engine parameters are described in Table 1, while the EcosimPro schematic and its component descriptions are proposed, respectively, in Fig. 1 and in Table 2.

Following the approach proposed in [22], let us define a stability map for the engine by performing simulations with variable injector pressure drops. Changing both fuel and oxidizer pressure drops, it is possible to create a map in which stable and unstable regions can be identified. The combustion inside the chamber is a rough process; hence, spontaneous oscillations in the pressure values are

Table 1 Main engine parameters

Parameter	Description	Meaning
D_c	Chamber diameter, cm	5.08
D_{th}	Throat diameter, cm	1.24
L^*	Characteristic length, m	2.31
L_c	Chamber length, cm	10.4
MR	Mixture ratio	5
p_c	Chamber pressure, bar	44.8
$\dot{m}_{\text{ox}}$	Mass flow rate, kg/s	0.249

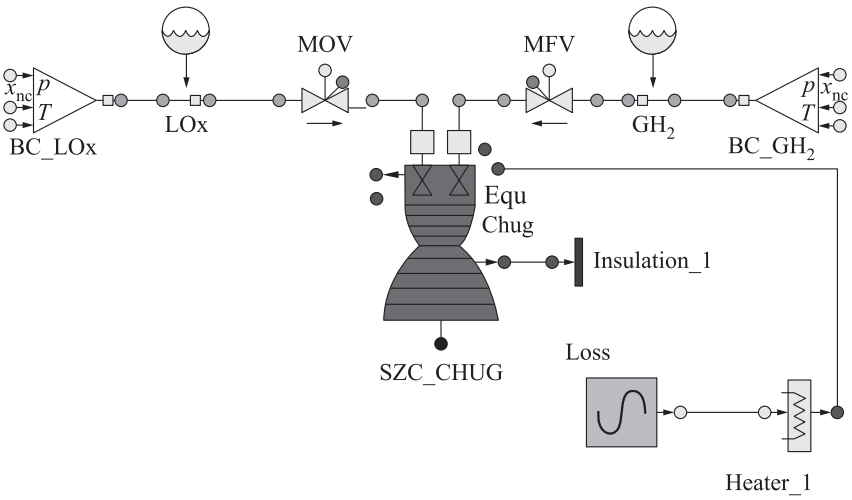

Figure 1 System schematic for chug analysis

Table 2 EcoosimPro component descriptions of Fig. 1

Component	Description
LOx/GH$_2$	Propellant definitions
BC_LOx/LH$_2$	Boundary conditions for propellant lines
MOV	Main oxidizer valve
MFV	Main fuel valve
Heater_1	Heat source
Loss	Heat losses time law
Insulation_1	Thermal insulation (zero heat flux)
SZC_CHUG	Combustion chamber

usually experienced. In order to mimic these oscillations and excite the chamber to eventually initiate the closed unstable loop between the camber and the upstream flow, we decided to introduce an unsteady term in the energy equation. The purpose here is to reproduce the combustion roughness, phenomena commonly identified as the exciting mechanism for combustion instabilities, by means of a broadband signal. The broadband reported in:

$$\dot{q}_{\text{unst}} = -\dot{q}_0 \left[1 + \epsilon \sum_{i=1}^{N} \sin\left(2\pi \left(f_0 + i\Delta f\right) t\right) \right] \tag{5}$$

f_0, Δf, N, and ϵ being, respectively, the first excited frequency, the sampling frequency, the number of samples, and the magnitude of the perturbation, precisely selects the frequencies of interest and, in the hypothesis of small perturbations, enables the analysis of the chamber response at the selected frequencies.

In this way, frequencies between f_0 and $f_0 + N\Delta f$ are excited every Δf. It is worth noticing that the broadband has a specific frequency content and periodicity characterizing its evolution in time. The steady value $\dot{q}_0$ is selected to mimic the losses measured in the combustion facility in order to match the experimental combustion efficiency $\eta_{c^*} = 0.75$. The final value is kept constant throughout all the simulations and equal to $\dot{q}_o = 1.933$ MW. This gives a low value of the combustion chamber temperature $T_c = 2038$ K as expected from the low combustion efficiency.

Pressure boundary conditions on both feed lines are changed throughout the simulations to ensure constant mass flow rates at steady state for different injectors pressure drops. It is worth saying that EcosimPro has its own component to ensure a constant mass flow rate in the feed line. This component could have been replaced in the schematic in Fig. 1 by both main oxidizer and main fuel valves, thus imposing the desired mass flow rates. However, it has been verified that the use of this component adds an artificial damping preventing the system from falling in any instability regime, hence failing in detecting chugging instabilities.

4 RESULTS

4.1 Constant Time Lag

In the case of constant time lag, the characteristic times are imposed as user input data. The values used here are inferred from the reference work [22]. In particular, the atomization time is, in this case, neglected and the vaporization lag is retrieved from the length needed to vaporize the 50 percent of the injected

liquid mass l_{50} [30]. Once the length is known, the vaporization time is calculated as the ratio of the vaporization length and the injection velocity of the liquid, $\tau_{\text{vap}} = l_{50}/v_{\text{inj}}$. Calculations for the examined engine configuration give a value of $\tau_{\text{vap}} = 4.4$ ms. The mixing and reaction times are then retrieved from the neutral stability condition. Starting from the experimentally observed chugging frequency at high injector pressure drops of 68 Hz, the phase requirement for stability gives an overall time delay of $\tau_{\text{tot}} = 6.7$ ms. Hence, the mixing time lag is obtained as a difference of the previously calculated delays $\tau_{\text{mix}} = 2.23$ ms.

The results obtained with the chugging module are here compared to those coming from both experimental evidences and Szuch's double time lag model. The tests are performed by fixing one of the two injector pressure drops, varying the other and measuring the response in terms of chamber pressure. The Root Mean Square (RMS) of the oscillations of the measured signal is then extracted and presented in terms of percentage values with respect to the mean chamber pressure, while the frequency content is analyzed by means of the signal Power Spectral Density (PSD). In this way, one is able to retrieve both amplitude of the response and characteristic frequencies of the system. It is worth noticing that the amplitude of the chamber response is strictly related to the amplitude of the input perturbation that, in turn, affects the definition of the stability region. In the experimental campaign, here referenced as [22], a 10 percent RMS criterion was used to identify stable and unstable operating regimes. In particular, all the configurations that give a pressure signal with a RMS exceeding the 10 percent of the mean chamber pressure value are considered unstable, while all the others can be considered stable.

The same consideration applies to the results coming from the simulation performed by Szuch *et al.* with the double time lag model. Furthermore, Szuch *et al.* imposed a white noise signal on the mean combustion products values to mimic the roughness of the combustion processes. The white noise input perturbation affects the entire spectrum but we are just interested in the lower part of the spectrum, since chug instabilities are associated with low frequencies. This consideration justifies the choice of a broadband input. In the subsequent analyses, the broadband signal in Eq. (5) is characterized by the values $f_0 = 0$, $\Delta f = 5$, $N = 20$, and $\epsilon = 0.01$. In Fig. 2, the results obtained with the chug module for both single and double time lag cases are compared with the results presented by Szuch *et al.* for both analog and experimental cases. In the single time lag case, only the injected liquid droplets are included in the chug module and are introduced with a time lag equal to the sum of vaporization, atomization, and mixing delays into the continuity equation. In the double time lag case, a delay equal to the mixing time lag is also imposed to the injected gaseous fuel. Results are obtained imposing a constant fuel injector pressure drop of $\Delta p_{\text{fu}}/p_c = 0.5$, varying the oxidizer injector pressure drops and measuring the pressure response in the chamber. Both of the methods (single and double time lag) are able to catch the increase in the RMS pressure values associated with

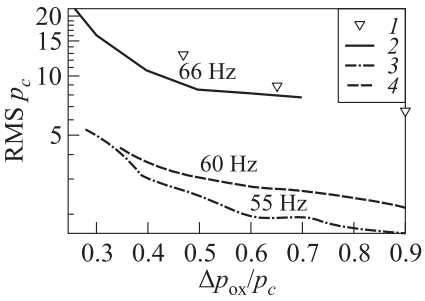

Figure 2 Double vs. single time lag, $\Delta p_{\text{fu}}/p_c = 0.5$; percentage chamber pressure RMS vs. oxidizer injector pressure drops: *1* — experimental; *2* — analog Szuch; *3* — single time lag; and *4* — double time lag

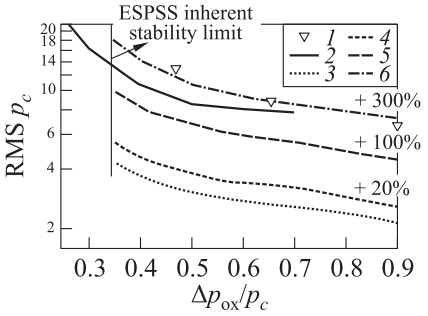

Figure 3 Double time lag, $\Delta p_{fu}/p_c = 0.5$: percentage chamber pressure RMS vs. oxidizer injector pressure drops at different input amplitudes: *1* — experimental; *2* — analog Szuch; *3* — $\epsilon = 0.01$; *4* — $\epsilon = 0.012$; *5* — $\epsilon = 0.02$; and *6* — $\epsilon = 0.04$

the reduction of pressure drops. This is a well-known behavior since increasing the injector pressure drops has a stabilizing effect on the overall system and decouples the oscillations in the feed lines of liquid oxygen from those in the combustion chamber, thus preventing the system from falling in the unstable regime. The predominant frequency resulting from the PSD in the single time lag case (55 Hz) differs from the one of the double time lag case (60 Hz). The result of this prediction has to be discussed considering that the broadband sampling frequency Δf introduces an uncertainty of ± 5 Hz.

The difference between the two approaches is related to the fact that in the double time lag, also, the fuel feed line couples dynamically with the oscillations in the combustion chamber, thus changing the phase relation between lines and combustion chamber. However, the small registered shift indicates that the chug frequency is mostly determined by the liquid oxygen, since the greater time lag is associated to this propellant and it dominates the phase relation between oscillations. Furthermore, in the single time lag case, the RMS values are always smaller than those of the double time lag approach and a plateau is observed between $\Delta p_{\text{fu}}/p_c = 0.6$ and 0.7. Furthermore, both time lag approaches give RMS values of the chamber pressure that are lower than those registered in the reference test cases. This is related with the amplitude ϵ of the broadband in Eq. (5).

In Fig. 3, the influence of the amplitude of the broadband signal on the chamber pressure is shown. Increasing the amplitude of the input perturbation increases the chamber pressure response and the values reported in the reference paper are approached. It must be noted that in the double time lag model, the

inherent stability limit is placed before the one reported in the reference work and this is true for all the selected level of amplitudes.

In both single and double time lag approaches, the system response to the broadband can be divided in three zones characterized by a different behavior in terms of both frequency content and signal shape. In Figs. 4 and 5, the time evolution of chamber pressure and the PSD of the same variable in the case of the double time lag model are, respectively, shown. Similar trends have been noted in the single time lag case. At high oxidizer pressure drops, the chamber pressure signal is proportional to the input signal, with a frequency content characterized by a small peak at 60 Hz. The frequency content is simply the one of the broadband perturbation and the dumping shown at this pressure drops must be considered as characteristic of the input signal instead of as system damping. When the oxidizer injector pressure drop is reduced, the 60-hertz frequency becomes predominant and the pressure signal assumes a characteristic damped behavior, now associated to the system. At $\Delta p_{\mathrm{fu}}/p_c = 0.35$, the system is still able to damp the perturbation and to prevent the oscillations from growing.

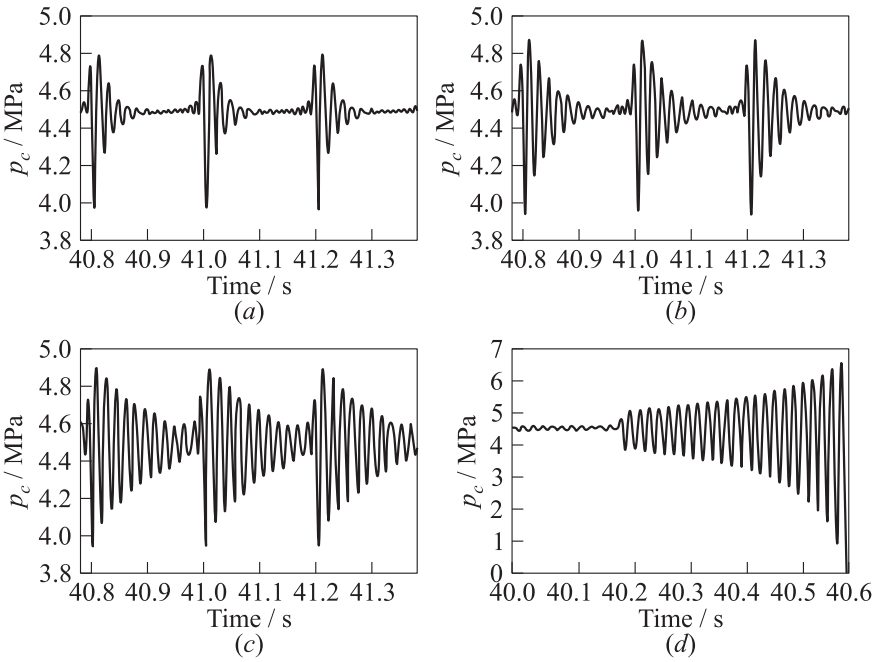

Figure 4 Double time lag, $\Delta p_{\mathrm{fu}}/p_c = 0.5$; time evolution of the chamber pressure response at different oxidizer injector pressure drops: (*a*) $\Delta p_{\mathrm{ox}}/p_c = 0.5$; (*b*) 0.4; (*c*) 0.35; and (*d*) $\Delta p_{\mathrm{ox}}/p_c = 0.3$, undamped case

No limit cycle is observed and the chamber pressure oscillations are damped and tend to disappear if not sustained with the input broadband signal. Below the inherent stability limit, $\Delta p_{\mathrm{ox}}/p_c < 0.35$, the system is not able to damp the oscillations, and the pressure response grows to high values causing the simulation to fail as shown in Fig. 4*d*. In this case, the system oscillates at the system characteristic frequency of 60 Hz and the oscillations are self-sustained even when the input is deactivated. Furthermore, the system oscillates at the characteristic frequency regardless the frequency content of the input, that is: the system diverges with a 60-hertz frequency even if a monochromatic input of 20 Hz is imposed for a short time and then deactivated.

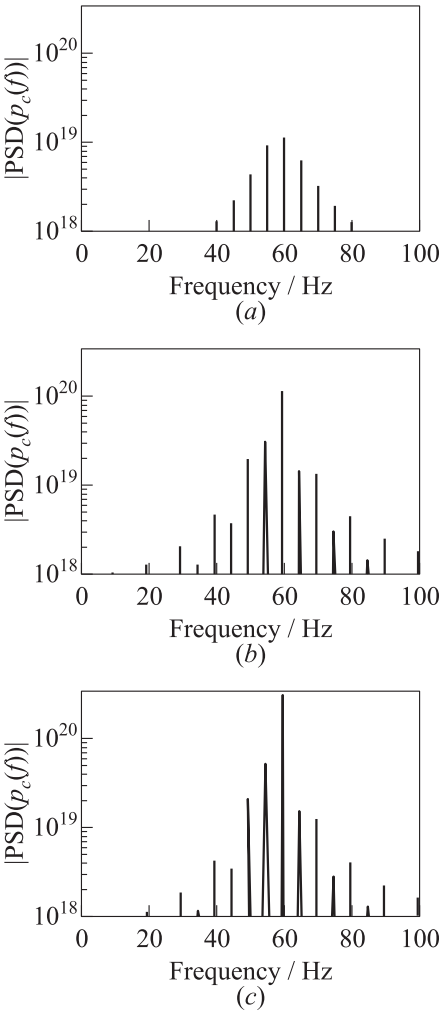

Figure 5 Double time lag, $\Delta p_{\mathrm{fu}}/p_c = 0.5$; PSD at different oxidizer injector pressure drops: (*a*) $\Delta p_{\mathrm{ox}}/p_c = 0.5$; (*b*) 0.4; and (*c*) $\Delta p_{\mathrm{ox}}/p_c = 0.35$

In Fig. 6, the stability map obtained for the selected test case with the double time lag model is shown. The results are compared with the boundaries identified by Szuch *et al.* It is worth noticing that the 10 percent RMS criterion is a practical criterion [22] to define a stability boundary. Since this criterion is directly related with the amplitude of the input perturbation, we choose to use a value of $\epsilon = 0.01$ throughout the simulations and we make use of also a 50 percent RMS criterion to identify the stability boundary. The boundaries identified with both the 10 and the 50 percent RMS criterion are shown with white dashed lines, whereas the reference results are shown in black. When the boundary is identified with the 50 percent criterion, the reversal in slope at lower $\Delta p_{\mathrm{fu}}/p_c$ is well matched, and, differently from the analog referenced computer program, no unstable regimes are identified at high oxidizer injector pressure drops when the

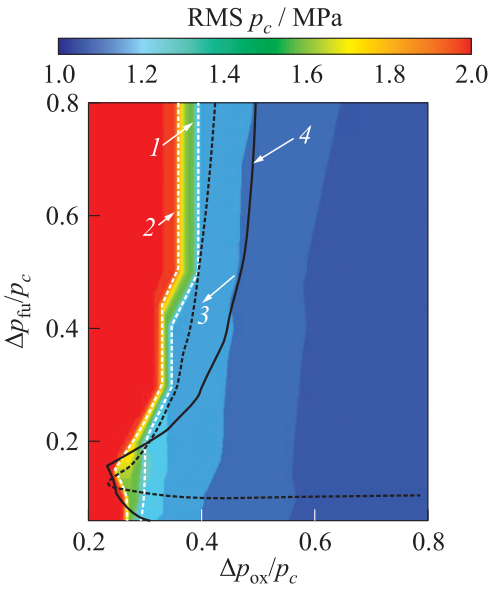

Figure 6 Stability map. Chamber pressure RMS dependency on oxidizer and fuel injector pressure drops: *1* — 10% RMS; *2* — 50% RMS; *3* — analog Szuch; and *4* — experimental

fuel injector pressure drop is lower than 0.15. The authors of the reference paper [22] justified this discrepancy assuming a backflow in the fuel injector element at lower pressure drops; however, this backflow has never been registered in our simulations. Furthermore, the reversal in slope is due to the intersection of two boundaries: the low-frequency boundary and the high-frequency boundary.

At lower fuel injector pressure drops, characteristic system frequencies ranging from 147 to 210 Hz were observed both experimentally and numerically [22]. In order to investigate the presence of this second frequency, we extend the broadband input up to 200 Hz, measuring the resulting chamber pressure signal. With this input, it is possible to register a higher frequency content of 175 Hz that is well within the limits of the aforementioned high-frequency range, giving a ratio of 2.9 between higher and lower frequency that well approximates the 2.7 ratio noted during multimode oscillations [31]. However, when the system enters its unstable regime at fuel injector pressure drops lower than 0.15, the pressure diverges with a frequency of 60 Hz, thus meaning that in our analysis, the 60-hertz frequency is the characteristic frequency of the system even at lower fuel injector pressure drops. Furthermore, PSD shows that the power associated to the 60-hertz component is always greater than the one at 175 Hz, explaining the predominance of the first frequency throughout the entire stability map.

For the constant time lag model, we finally investigate the influence of different input amplitudes for various fuel pressure drops. The scope is here to investigate how the stability boundaries are influenced by the level of the input perturbations. In particular, the results obtained when the amplitude ϵ in Eq. (5) is increased of 20% and 100% are presented. The results in terms of the RMS of chamber pressure oscillations are then normalized with those obtained with the reference case $\epsilon = 0.01$ and divided by the respective percentage increment. In this way, we are able to understand whether the response of the system is

linear. In fact, in the case of a linear behavior, the plots should be equal to 1 for all the selected cases, whereas the differences show the presence of nonlinearities related to the effect of the injector pressure drops. In particular, for each of the fuel pressure drops, the response is about 20% higher at higher oxidizer pressure drops and is nearly linear in the lower oxidizer pressure drops domain. Furthermore, this trend indicates that the relative increase with respect to the reference test case with $\epsilon = 0.01$ is not affected by the amplitude of the input noise (both for $\epsilon = 0.012$ and 0.02). Considering as example the points with $\Delta p_{\text{ox}}/p_c = 0.8$ and $\Delta p_{\text{fu}}/p_c = 0.4$ in Fig. 7*c*, one may find that the absolute root mean square values are 1.34 and 2.47 bar, respectively, for $\epsilon = 0.012$ and 0.02, both showing a linear trend with respect to the 1.08-bar value obtained in the $\epsilon = 0.01$ case. Therefore, the system shows that the pressure response to the input noise is nearly linear. Nevertheless, there are no experimental measures in the referenced paper for RMS values below 6 bar ($\approx$ 13% of the operative pressure) (see Fig. 3), thus not providing any validation point for the model.

However, it must be pointed out that the amplitude of pressure oscillations is such that nonlinear effects could be activated for these levels of input noise.

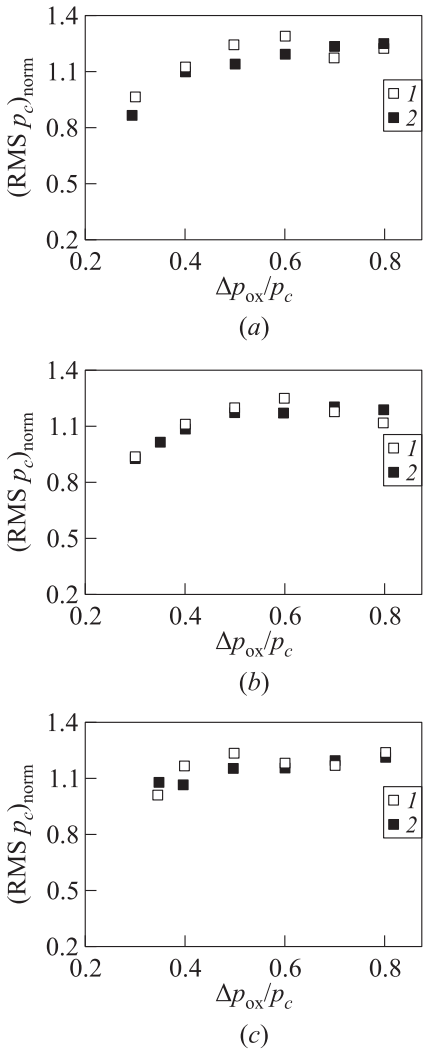

Figure 7 Double time lag; normalized RMS of the chamber pressure signal for different input amplitudes (*1* — +20% and *2* — +100%) at various fuel injector pressure drops: (*a*) $\Delta p_{\text{fu}}/p_c = 0.1$; (*b*) 0.15; and (*c*) $\Delta p_{\text{fu}}/p_c = 0.4$

Furthermore, the results shown in Fig. 7 highlight that for different fuel injector pressure drops, the system response has a maximum at higher oxidizer injector pressure drops. Therefore, when the amplitude of the input perturbation is increased, the boundary of the stability regions experiences a greater shift if placed in the high-pressure drop

region and a smaller shift if placed in the low-pressure drop region. It should be noted that increasing the input amplitude does not affect the characteristic frequency of the system that remains equal to 60 Hz.

4.2 Variable Time Lag

The time lags are typically not known *a priori*; hence, when a new engine configuration is analyzed, it is useful to retrieve the needed time delays by means of dedicated correlations. The benefit of introducing correlations for the time lags is dual: on one hand, the user is free from any *a priori* calculation of the time lags and, on the other hand, the time lags become time-varying functions of the combustion chamber variables. In this frame, we introduced semiempirical correlations to calculate atomization and vaporization time lags, considering the combustion as sufficiently fast. As mentioned in paragraph 2.1.3, the time lags for atomization and vaporization processes are retrieved, respectively, from Eqs. (3) and (2), while mixing time lag is evaluated from an empirical curve [14]. A double time lag approach is still used; hence, the total time delay for the liquid oxygen is retrieved as the sum of vaporization, atomization, and mixing time lags while only the mixing time lag characterizes the gaseous hydrogen delay. Some considerations must be done on the correlation for the initial droplet diameter Eq. (4). Due to the lack of informations on the experimental setup, the recess of the oxidizer post R_{post} is an unknown data that greatly influences the value of the initial droplet diameter and, in turn, the vaporization time. Furthermore, the injector coefficient C_{inj} can range from 0.4 to 1.2, thus changing significantly the vaporization delay. We know, from experimental evidences [28], that the initial droplet diameters of liquid oxygen at high pressure range from 60 to 160 μm. Hence, stated that the recess length is a construction parameter of a few millimeters, we decided to use a combination of values that, while respecting all of the aforementioned constraints, ensures a vaporization time lag at steady state equal to $\tau_{\text{vap}} = 4.4$ ms. In this way, we retrieved a time varying time lag matching with the steady-state values suggested from the experimental evidences [22]. The chosen reference working point is characterized by the values $R_{\text{post}} = 0.003$, $C_{\text{inj}} = 0.4$, and $K = 0.121$.

The time-dependent approach is then tested on the engine configuration presented in section 3. A single fuel injector pressure drop is here investigated at different oxidizer injector pressure drops and results are compared in Fig. 8 against those obtained for the constant time lag approaches. The variable time lag approach gives a pressure response in line with the fixed time lag approaches. The amplitudes of the oscillations are less influenced by the reduction of the oxidizer injector pressure drop and a smoother growth is observed while passing from high to low injector pressure drops. Finally, the time-dependent time lags give a characteristic frequency of 65 Hz approaching the experimental measured

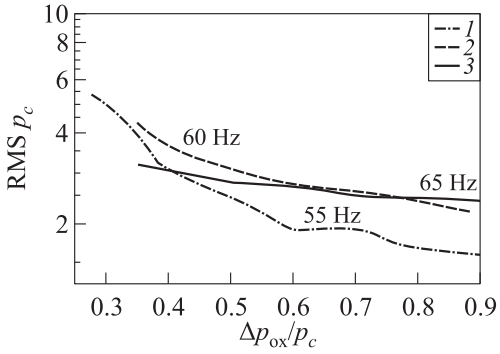

Figure 8 Double time lag, $\Delta p_{fu}/p_c = 0.5$; chamber pressure RMS vs. oxidizer injector pressure drops: *1* — constant single time lag; *2* — constant double time lag; and *3* — variable double time lag

value of 68 Hz, with an uncertainty of 5 Hz related to the broadband sampling frequency. Furthermore, the tendency of the double time lag approach in anticipating the insurgence of the inherent stability limit is here confirmed. In fact, in both double time lag approaches, the limit moves towards higher oxidizer pressure drops and for pressure drops lower than $\Delta p_{ox}/p_c = 0.23$ the system is not able to damp the imposed perturbation causing the chamber pressure to diverge with a frequency equal to the characteristic frequency of 65 Hz.

5 CONCLUDING REMARKS

A double time lag model to investigate low-frequency combustion instabilities has been implemented in the system analysis tool EcosimPro and tested against experimental results. Two different approaches have been followed: a constant time lag and a variable time lag approach based on semiempirical correlations. The constant time lag approach demonstrates its effectiveness in reproducing the unstable behavior associated with the reduction of the injector pressure drops, in particular, no stable region has been identified for an oxidizer injector pressure drop lower than 0.35. The chug module is able to reproduce the reversal in slope of the stability boundary at low injector pressure drops, thus giving a result close to the one found in the reference experiment. However, it must be pointed out that the location of the stability boundary depends on both the criterion used to identify a regime as unstable and on the amplitude of the input perturbation. It is demonstrated that the boundaries can be easily shifted by changing the amplitude of the input perturbation and that this shift slightly

depends on the selected injector pressure drop. Hence, in the computer program, the stability boundaries can be shifted in accordance with the level of the input perturbation. Despite its simplicity, the constant time lag approach is able to predict a characteristic frequency close to the one measured experimentally.

The registered high-frequency content is characterized by a ratio of higher to lower frequency close to 2.7, as reported in open literature. It must be noted that in the described case, high frequency does not dominate the dynamic response at low fuel injector pressure drops and the instability is still related to the first characteristic frequency. The inability in catching the suppression of the first mode could be related with a lack of data for parameters that usually influences the damping effect and the associated system impedances, i. e., injector cavity volumes and length of the feed lines. These values have been selected to be consistent with the downstream injector geometry and mass flow rates, but a fine tuning with the real data is unavoidable to improve the results of the model. The chugging module has been finally tested with semiempirical correlations to retrieve characteristic delays that, depending on the main flow variables, are time-dependent functions of the main combustion chamber parameters. With the implemented correlations, the model retrieves a lower characteristic frequency that better approximates the experimental results, while the predicted RMS values of the chamber pressure remain comparable with those obtained with the constant double time lag model.

ACKNOWLEDGMENTS

The work was conducted in the frame of the Network Partnering Initiative agreement between the European Space Agency (ESA) and the Dipartimento di Ingegneria Meccanica e Aerospaziale (DIMA) of 'La Sapienza' University of Rome.

REFERENCES

1. Gunder, D. F., and D. R. Friant. 1950. Stability of flow in a rocket motor. *J. Appl. Mech. ASME T.* 17(3):327–333.
2. Summerfield, M. 1951. A theory of unstable combustion in liquid propellant rocket systems. *J. Am. Rocket Soc.* 21(5):108–114.
3. Crocco, L. 1951. Aspects of combustion stability in liquid propellant rocket motors part I: Fundamentals. Low frequency instability with monopropellants. *J. Am. Rocket Soc.* 21(6):163–178.
4. Wenzel, L. M., and J. R. Szuch. 1965. *Analysis of chugging in liquid-bipropellant rocket engines using propellants with different vaporization rates.* National Aeronautics and Space Administration.

5. Casiano, M. J. 2010. Extensions to the time lag models for practical application to rocket engine stability design. The Pennsylvania State University. PhD Thesis.
6. Webber, W. T. 1972. Calculation of low-frequency unsteady behavior of liquid rockets from droplet combustion parameters. *J. Spacecraft Rockets* 9(4):231–237.
7. Bartrand, T. A. 1987. A study of low frequency combustion instability in rocket engine preburners using a heterogeneous stirred tank reactor model. Knoxville, TN: University of Tennessee. PhD Thesis.
8. Empresarios Agrupados. 2007. EcosimPro. Available at: http://www.ecosimpro.com (accessed February 13, 2018).
9. De Rosa, M., J. Steelant, J. Moral, and R. Perèz. 2010. ESPSS simulation platform. *Space Propulsion Conference*. San Sebastian, Spain.
10. Di Matteo, F., and J. Steelant. 2014. *Multi-disciplinary propulsion simulations at engineering level by means of the European space propulsion system simulation ESPSS*. RTO/AVT/VKI lecture ser. on fluid dynamics associated to launcher developers. St. Genesius-Rode, Belgium: Von Karman Institute. 318 p.
11. Crocco, L. 1952. Aspects of combustion stability in liquid propellant rocket motors. Part I: Low frequency instability with bipropellants. High frequency instability. *J. Am. Rocket Soc.* 22(1):7–16.
12. Crocco, L., and S.-I. Cheng. 1956. *Theory of combustion instability in liquid propellant rocket motors*. Cambridge University Press. 200 p.
13. Szuch, J. R. 1969. Application of a double-dead-time model describing chugging to liquid propellant rocket engines having multielement injectors. Technical Note TN D-5303. NASA.
14. Szuch, J. R. 1970. Digital computer program for analysis of chugging instabilities. Washington, D.C.: National Aeronautics and Space Administration. 76 p.
15. Harrje, D. T., and F. H. Reardon. 1972. Liquid propellant rocket combustion instability. NASA Special Publication 194.
16. Ordonneau, G., N. Girard, and N. David. 2000. Analysis and modeling of Vulcain engine shutdown transient chugging. Office National d'etudes et de recherches aerospatiales ONERA-PUBLICATIONS-TP No. 143.
17. Ordonneau, G., F. Levy, and N. Girard. 2001. Low frequency oscillation phenomena during VULCAIN shutdown transient. *37th AIAA/ASME/SAE/ASEE Joint Propulsion Conference and Exhibit*. Salt Lake City, UT.
18. Fang, J. 1984. Application of combustion time-lag theory to combustion stability analysis of liquid and gaseous propellant rocket engines. *22nd AIAA Aerospace Sciences Meeting*. Reno, NV.
19. Sirignano, W. A., J. P. Deplanque, C. H. Chiang, and R. Bhatia. 1995. Liquid-propellant droplet vaporization: A rate-controlling process for combustion instability. *Liquid rocket engine combustion instability*. Eds. V. Yang and W. E. Anderson. Progress in astronautics and aeronautics ser. 169:307–343. doi: 10.2514/5.9781600866371.0307.0343.
20. Boronine, E., K. Vollmer, and M. Frey. 2013. A modified ESPSS combustion chamber model with chugging modeling capability. *2nd ESPSS Workshop, ESTEC*. Noordwijk, The Netherlands.

21. Vingert, L., P. Gicquel, M. Ledoux, I. Carré, M. Micci, and M. Glogowski. 2004. Atomization in coaxial-jet injectors. *Liquid rocket combustion instability*. Ed. V. Yang. Progress in astronautics and aeronautics ser. 200:105–140.
22. Szuch, J. R., and L. M. Wenzel. 1967. Experimental verification of a double-dead-time model describing chugging in liquid-bipropellant rocket engines. NASA. Technical Report.
23. Di Matteo, F. 2012. Modelling and simulations of liquid rocket engine ignition transients. University of Rome "La Sapienza." PhD Thesis.
24. Bruce Stewart, H., and B. Wendroff. 1984. Two-phase flow: Models and methods. *J. Comput. Phys.* 56(3):363–409.
25. Ranz, W. E., and W. R. Marshall. 1952. Evaporation from drops. *Chem. Eng. Prog.* 48(3):141–146.
26. Meng, H., G. C. Hsiao, V. Yang, and J. S. Shuen. 2005. Transport and dynamics of liquid oxygen droplets in supercritical hydrogen streams. *J. Fluid Mech.* 527:115–139.
27. Yang, V. 2001. Liquid-propellant droplet combustion and cluster-behavior at supercritical conditions. DTIC Document. Technical Report.
28. Lafon, P., H. Meng, V. Yang, and M. Habiballah. 2007. Vaporization of liquid oxygen (LOx) droplets in hydrogen and water environments under sub- and supercritical conditions. *Combust. Sci. Technol.* 180(1):1–26.
29. Ferrenberg, A. J., and M. S. Varma. 1984. Atomization data requirements for rocket combustor modeling. *21st APL JANNAF Combust. Meeting*. 1:369–377.
30. Priem, R. J., and M. F. Heidmann. 1960. Propellant vaporization as a design criterion for rocket-engine combustion chambers. National Aeronautics and Space Administration. Vol. 67.
31. Anon. 1962. J-2 Program Quarterly Progress Report for Period Ending February 28, 1962. Rocketdyne Div. North American Aviation. Technical Report No. R-2600-6(NASA CR-63323). P. 85, 137–140.